Ceramics International 51 (2025) 43924–43932

Contents lists available at ScienceDirect

Ceramics International

journal homepage: www.elsevier.com/locate/ceramint

Mutually enhanced mechanical and tribological properties in magnetron sputtered Mo_2N/Ag-SiN_x self-lubricating multilayered films via epitaxial growth design

Jing Luan [a,b], Lei Wang [a], Songtao Dong [a], Filipe Fernandes [b,c], Andrei Choukourov [d], Junfeng Yang [e], Mitjan Kalin [f], Albano Cavaleiro [b], Hongbo Ju [a,b,f,*]

[a] Jiangsu University of Science and Technology, School of Materials Science and Engineering, Mengxi Road 2, Zhenjiang, Jiangsu Province, 212003, China
[b] University of Coimbra, CEMMPRE, ARISE, Department of Mechanical Engineering, Rua Luís Reis Santos, 3030-788, Coimbra, Portugal
[c] CIDEM, ISEP - Polytechnic of Porto, Rua Dr. António Bernardino de Almeida, 4249-015, Porto, Portugal
[d] Charles University, Faculty of Mathematics and Physics, Department of Macromolecular Physics, V Holesovickach 2, Prague, 180 00, Czech Republic
[e] Key Laboratory of Materials Physics, Institute of Solid State Physics, Hefei Institutes of Physical Science, Chinese Academy of Sciences, Hefei, 230031, China
[f] University of Ljubljana, Faculty of Mechanical Engineering, TINT - Laboratory for Tribology and Interface Nanotechnology, Aškerčeva 6, 1000, Ljubljana, Slovenia

ARTICLE INFO

Handling Editor: Dr P. Vincenzini

Keywords:
Magnetron sputtering
Mo_2N/Ag-SiN_x multilayered films
Coherent strengthening
Mechanical properties
Tribological properties

ABSTRACT

Achieving simultaneous enhancement of both mechanical and self-lubricating properties by incorporating soft lubricants into nitride films has been a longstanding challenge in the development of solid lubricant materials. This paper introduced a novel approach to overcome this challenge by developing coherent-structured Mo_2N/Ag-SiN_x multilayered films using radio frequency (RF) magnetron sputtering. The multilayer films were designed with a fixed modulation period of 30 nm, while the modulation ratio (γ) was varied from 1:9 to 1:1. The Mo_2N layers exhibited a single fcc-Mo_2N phase, while the Ag-SiN_x layers formed a dual-phase structure comprising fcc-Ag nanoparticles embedded in an amorphous SiN_x matrix. At a modulation ratio of 1:9, the Ag-SiN_x layer epitaxially grew on the Mo_2N template, resulting in a coherent structure. This coherent structure significantly enhanced both the hardness and elastic modulus, reaching approximately 36 GPa and 230 GPa, respectively. The improved wear resistance at room temperature can be attributed to the coherent strengthening effect, which not only elevated the film's hardness but also eliminated sharp interfaces between modulation layers, thereby reducing crack initiation sites. In temperature-cycling tribo-testing from room temperature to 600 °C, the film with a γ of 1:9 maintained a stable coefficient of friction around 0.2, except during the initial room temperature, where it was 0.4. The wear rate could not be accurately calculated due to the adhered tribolayer on the top of the wear track following the initial tribo-test at 600 °C. The excellent tribological properties across temperature cycles were attributed to the synergistic lubricant characteristics of both layers and the formation of self-lubricating tribo-phases. The optimized Mo_2N/Ag-SiN_x multilayered films provide an effective balance of lubrication and mechanical stability under extreme conditions, making them highly promising for high-performance engineering applications.

1. Introduction

Over the past few decades, the development of wide-range temperature self-lubricant films has emerged as a pivotal focus in the field of surface engineering. These films are designed to meet the rigorous demands of critical applications, such as high-performance machining and aerospace technology [1–3]. The introduction of the classical "self-adaptation" principle marked a turning point, considerably accelerating the innovation and refinement of multi-component self-lubricating film materials [4,5].

Magnetron sputtering technology has enabled the incorporation of soft metals such as Ag, Cu, and Ni into hard matrices such as TiN [6,7], NbN [8,9], VN [10,11], and Mo_2N [12,13], resulting in films that maintain excellent self-lubricant properties across a broad temperature

* Corresponding author. Jiangsu University of Science and Technology, School of Materials Science and Engineering, Mengxi Road 2, Zhenjiang, Jiangsu Province, 212003, China.
E-mail addresses: hbju@just.edu.cn, hju@uc.pt (H. Ju).

https://doi.org/10.1016/j.ceramint.2025.07.123
Received 18 May 2025; Received in revised form 27 June 2025; Accepted 10 July 2025
Available online 12 July 2025

spectrum. What's more, the MoN/Ag coating with 2.2 % Ag had excellent tribological properties [12]. The effectiveness of these kinds of films is largely ascribed to two key mechanisms: (i) the soft metals exhibit superior lubricant properties at medium to high temperatures [12–14]; and (ii) the combination of soft metals and hard nitride matrices facilitates self-lubricant frictional chemical reactions across various temperatures, producing unique self-lubricant phases [15–17]. Despite of these advancements, significant challenges persist: (i) achieving effective self-lubricant across a wide range of temperatures requires an optimal concentration of soft metals; however, when these kinds of metals are dispersed within a hard matrix, they often compromise the mechanical strength of the films; (ii) excessive diffusion of soft metals at elevated temperatures reduces the ability to maintain consistent lubrication, leading to the premature failure of the films' long-term lubricating properties. These issues have significantly hindered the widespread adoption of these films in the industry.

To address the existing limitations of the inversion between the lubricant and mechanical properties in this kind of films, two prevalent approaches have been employed: (i) alloying the films with other metal/nonmetal elements to improve the overall hardness of the films [18–20], and (ii) reducing the relative content of soft metals to achieve an optimal balance between lubricant and mechanical properties [21–23]. To overcome the rapid diffusion of the lubricant agents, anti-diffusion phases/layers are incorporated into the self-lubricant matrix for achieving the long-term lubrication at elevated temperatures. For instance, an amorphous SiN_x phase has been used either as a distinct layer in the multilayered structure or as a three-dimensional encapsulation around the lubricant phase, effectively controlling or even blocking the diffusion of the lubricant agents [20,24,25]. Nevertheless, this architecture design approach may compromise the wide temperature range self-lubricant performance to some extent.

Achieving a balance between long-term self-lubrication across a wide range of temperatures and maintaining the overall mechanical properties of solid lubricant films remains a significant challenge. In a recent work, the authors of this paper have highlighted the mechanisms that contribute to strengthening in ceramic-based thin films containing very low levels of soft metals (<5 at.%), with coherent strengthening identified as a key mechanism that significantly enhances the overall mechanical resilience and performance of these advanced films [51]. Additionally, we integrated nanocrystalline Ag into an amorphous SiN_x matrix by utilizing magnetron sputtering technology, enabling precise control and continuous release of Ag in high-temperature environments. Through precise optimization of the film alloy composition, we successfully achieved a delicate balance between lubricant agents' diffusion and anti-diffusion [27].

Building upon the aforementioned research foundation, the present paper introduces a novel film system - Mo_2N/Ag-SiN_x, which is designed to achieve long-term lubrication capabilities while simultaneously ensuring the overall outstanding mechanical properties of the film. The architecture is developed to: (i) the incorporation of the amorphous SiN_x phase is employed to facilitate the continuous release of Ag and to provide protection to Mo_2N in high-temperature environments, thereby improving the film's capability to withstand temperature cycling variations during wear tests; (ii) through the meticulous optimization of the thickness of the two modulation layers, we induce coherent growth of Ag and Mo_2N template layers, leveraging coherent strengthening to significantly enhance the overall mechanical properties of the film.

To accomplish these objectives, this study employs magnetron sputtering technology to meticulously incorporate high-performance Mo_2N and Ag-SiN_x as modulation layer materials. We design and fabricate a series of nanostructured multilayer films, Mo_2N/Ag-SiN_x, by maintaining a fixed modulation period and varying the modulation ratio. The study investigates how the modulation ratio influences the film's mechanical properties, friction, and wear characteristics, particularly under temperature cycling conditions ranging from room temperature up to 600 °C. The ultimate goal is to optimize the structural characteristics of the film and to elucidate its tribological performance across a broad temperature range based on the ratio of the two modulation layers.

2. Experimental information

A series of Mo_2N/Ag-SiN_x multilayered films was prepared using RF magnetron sputtering, from high purity (99.9 %) Mo, Si and Ag targets. Reference films with single monolithic architecture, i.e. individual Mo_2N [28,29] and Ag-SiN_x [27] films were produced for study of the morphology, composition and structure of individual layers in the multilayer films. Polished high-speed steel W18Cr4V (W18) and Si (100) wafers were used as substrates in the depositions. Before depositions the substrates were ultrasonically cleaned in alcohol for 15 min and propanol for 15 min. High-speed steel substrates were used for mechanical and tribological properties evaluation (hardness, elastic modulus and tribological assessment, either at room temperature (RT) and temperature cycling conditions (RT-600C°, repeated different times), whilst Si substrates were used for X-ray diffraction (XRD), and transmission electron microscopy (TEM) analyses. The distance between the targets and substrates was set to 80 mm. Prior to the depositions, the chamber was vacuumed down below 6.0×10^{-4} Pa. A Mo adhesion layer with thickness 150 nm was firstly deposited under Ar flow of 10 sccm in order to improve the adhesion of the films to the substrate. After that, the multilayer structure was deposited by opening the Mo shutter and closing the shutters of the Si and Ag target, in alternated way, in the presence of a N_2 atmosphere. The multilayered structure was grown by applying a power 280, 150 and 50 W at the Mo, Si and Ag targets, respectively, in all the depositions. The Ar and N_2 partial pressures were 0.23 and 0.07 Pa, corresponding to a total working pressure of 0.3 Pa. Films with different modulation ratios (ratio of thickness of Ag-SiN_x to Mo_2N) ranging from 1:9 to 1:1 with a fixed modulation period (the thickness of the layer of Mo_2N and its adjacent Ag-SiN_x) of 30 nm, were produced by controlling the sputtering time from the Mo, Ag and Si targets. Schematic diagram of the deposition system for sputtering modulation layers is shown in Fig. 1.

The crystal structure of Mo_2N/Ag-SiN_x films was determined by X-ray diffraction (XRD, Shimazu-6000, Shimadzu, Kyoto, Japan) with Cu Kα radiation at a pass energy of 160 eV, in a 2 θ interval ranging from 20 to 80° with a step of 4°/min. The microstructure of the films was investigated by the transmission electron microscope (TEM, JEOL, JEM-2100F, Japan) with an accelerate voltage of 200 kV. Hardness (H) and elastic modulus (E) was measured by the nano-indentation (Anton Paar, CPX + NHT2 + MST, Switzerland), setting the constant loading force to 3 mN and holding time of 10 s. 0.1 mN/s was applied for the loading and unloading speed during the measurement. Nano-indentation measurements were conducted on two distinct zones of each specimen, with fifteen measurements taken in each zone. The average value was then calculated from those thirty measurements to ensure the accuracy and reliability of the mechanical testing. The ball-disk tribo-tester (UMT, UMT-2, CETR, USA) was applied to investigate the tribological properties at room temperature (RT) and RT-600 °C temperature-cycling. The wear test was carried at a speed of 50 rpm at RT, for 30 min under a normal load of 5 N with a counterpart of alumina ball with a diameter of 9.5 mm. The relative humidity was about 30 % during the tribo-testing at RT. Data from the steady state zone of the friction curve was calculated as average coefficient of friction. The wear test was repeated three times to ensure data reliability. The temperature-cycling (RT and 600 °C) tribological behavior of the selected specimen, which exhibited the best RT tribological performance, was evaluated using the same ball-disk tribo-tester. Initially, the specimen underwent RT tribo-testing for 20 min (RT-1) under the same parameters used in the initial RT one. Subsequently, the specimen was heated up to 600 °C for the first elevated tribo-test (600-1) and the test conducted at the same wear track, using a 5 N load with an alumina counterpart for 20 min. The combination of RT-1 and 600-1 constituted one unit of the temperature-

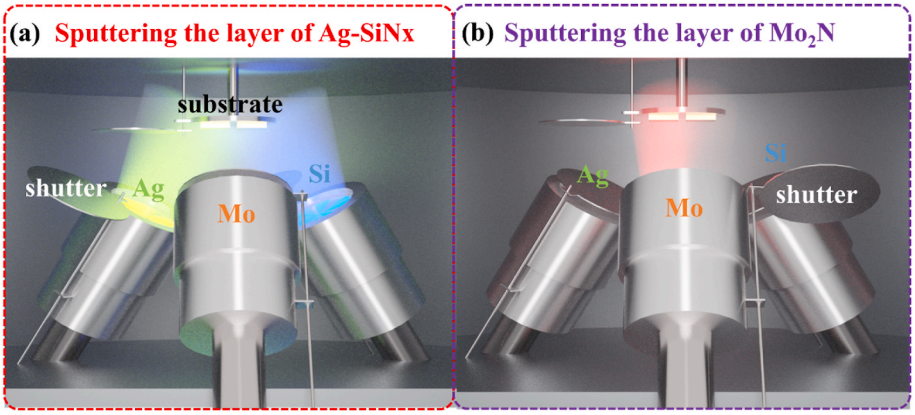

Fig. 1. Schematic diagram of the deposition system: (a) Ag-SiN_x layer and (b) Mo_2N layer.

cycling tribo-test, which was repeated three times to thoroughly investigate the specimen's tribological behavior under the RT-600 temperature cycling. The Raman spectrum of inside and outside of wear tracks were obtained by Raman spectrometry (inVia, Renishaw, UK). The average cross section area of wear tracks test was measured by 2D Profilometry (BRUKER, Dektak-XT, Germany), and the wear rates of these films were obtained by combining the calculation formula [3].

3. Results and discussion

3.1. Microstructure

Fig. 2 depicts the XRD patterns of the reference Mo_2N and Ag-SiN_x monolayered films, and the Mo_2N/Ag-SiN_x multilayered films. The monolayered Mo_2N film exhibits six diffraction peaks at approximately at 37, 43, 63, 69, 74, and 79°, corresponding to fcc-Mo_2N (111), (200), (220), silicon wafer substrate, (311), and (222), respectively. Then, the film exhibits only a single phase of fcc-Mo_2N. Four diffraction peaks could be observed in the pattern of Ag-SiN_x monolayered film, located at around 38, 44, 64 and 69.2°. These peaks can be indexed as the fcc-Ag (111), (200), (220) planes, and the silicon wafer substrate, respectively. No any other diffraction peaks from crystalline SiN_x appears in this XRD diffraction pattern, suggesting the total amorphous state of the SiN_x in the film. This result agrees well with the previous published paper on Ag-SiN_x films with a microstructure of nano-particles of Ag

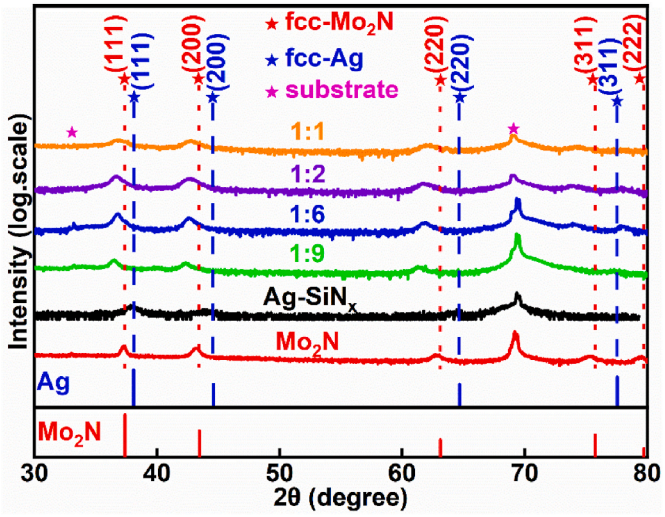

Fig. 2. XRD diffraction patterns of the Mo_2N, and Ag-SiN_x monolayered films, and the Mo_2N/Ag-SiN_x multilayered films as a function of modulation ratio of Ag-SiN_x to Mo_2N thickness.

embedded into an amorphous SiN_x matrix [27]. Consequently, the Ag-SiN_x monolayered film exhibits a dual-phase of fcc-Ag and amorphous SiN_x phase.

In the multilayered system with a modulation ratio of 1:9, the diffraction peaks closely resemble those of the reference Mo_2N monolayered film, though they exhibit a noticeable shift toward lower angles. As the modulation ratio increases, the multilayer film continues to exhibit six diffraction peaks, five of which matches well the peaks of the single fcc-Mo_2N. Compared to the multilayered film with a 1:9 modulation ratio, these peaks exhibit slight asymmetry and a minor shift toward higher angles, even though the diffraction peaks observed in the Mo_2N monolayered film consistently shift to the left.

The observed low-angle shift in the diffraction peaks is likely related to the residual stress and interface characteristics within the multilayered film. The Mo_2N monolayered reference film was characterized by a residual compressive stress with a value of around −1.0 GPa [28–32]. Residual stress in nitride-based films is highly dependent on its thickness, with compressive stress sharply increasing as the thickness decreases [33–35]. In the case of the multilayer films, although the overall film thickness remains stable at approximately 2 μm, the alternating deposition of Mo_2N and Ag-SiN_x layers disrupts the continuous growth of the Mo_2N layer and, thereby resulting in a significantly higher residual compressive stress in the Mo_2N layers of the multilayer film compared to the monolayer reference one, which primarily accounts for the leftward shift in the diffraction peaks. Additionally, the coherent structure of Ag within the Ag-SiN_x layers, facilitated by epitaxial growth on the Mo_2N template in the multilayer film with a 1:9 modulation ratio (as confirmed latter by the TEM analysis), leads to a reduction in the plane spacing of Mo_2N near to the interfaces. Consequently, it further intensifies the residual compressive stress in the Mo_2N layer, causing the diffraction peak to shift even further to the left. However, as the modulation ratio increases, the disappearance of this coherent structure leads to a slight reduction in the residual compressive stress within the Mo_2N layer. Moreover, the thicker Ag-SiN_x layers could contribute to a higher overall thermal expansion coefficient for the multilayer film, given that Ag exhibits a greater thermal expansion coefficient as compared to nitrides [24,25,36]. This induces additional tensile stress due to the thermal expansion [36–39], which partially offsets the compressive residual stresses. For the multilayered film other than the one with a 1:9 modulation ratio, residual stress results from a of various competing factors, including thermal expansion, interface characteristics, and the thickness of the Mo_2N layer. Consequently, while the diffraction peaks of the multilayer films remain consistently shifted to the left of the Mo_2N monolayer reference, significant shifts in peak positions are not observed with varying modulation ratios.

Regarding the shape of the diffraction peaks from the as-deposited multilayered films, the film with a 1:9 modulation ratio exhibits a coherent structure characterized by the epitaxial growth of Ag on the

Mo_2N template, as confirmed by TEM image (Fig. 3). This epitaxial characteristic results in an expansion of the Ag plane spacing, leading to a symmetric diffraction peak. However, the formation of this epitaxial structure is highly dependent on the thickness of the modulation layers. Once the thickness exceeds a critical value, the coherent structure rapidly disintegrates. As a result, the diffraction peaks from both Mo_2N and Ag begin to overlap, contributing to each peak in the XRD pattern. The close proximity of the Mo_2N and Ag peaks leads to an asymmetric shape in the diffraction peaks, as observed in Fig. 1.

Fig. 3 shows the TEM results from the cross-sectional Mo_2N/Ag-SiN_x multilayered specimen with a modulation ratio of 1:9. The cross-sectional TEM image, depicted in Fig. 3(a), exhibits alternating layers of Mo_2N (dark) and Ag-SiN_x (light). The thickness of Mo_2N and Ag-SiN_x layer are approximately 27 and 3 nm, respectively, as shown in the enlarged inset in Fig. 3(a). This result is in good agreement with the designed modulation ratio/period.

The selected area electronic diffraction (SAED) pattern from the zone A in Fig. 3(a) is shown in Fig. 3(b). This pattern displays five distinct diffraction rings, in addition to the central transmission spot. However, these rings are challenging to differentiate because their measured values fall between those of the fcc-Mo_2N and fcc-Ag planes. This observation differs from the results obtained through XRD patterns. The diffraction peaks in XRD primarily arise from planes within the film that are parallel to the surface, which are highly susceptible to stress—both intrinsic and thermal—during deposition and cooling. Unlike bulk materials, the films studied here exhibit a 2D-like structure, where stress significantly impacts the sample parallel to the surface. In contrast, the SAED pattern, derived from a cross-sectional specimen, reflects the crystal characteristics perpendicular to the surface. The epitaxial growth of Ag on the Mo_2N template leads to a contraction of Mo_2N planes at the interfaces and an expansion of Ag planes, as illustrated in Fig. 3(c). This interaction results in plane spacings that, as calculated from the diffraction rings in Fig. 3(b), fall between those of the fcc-Mo_2N and fcc-Ag planes.

Fig. 3(c) shows the high-resolution TEM (HRTEM) image from the inset in Fig. 3(a). A clear interface between the layers of Mo_2N and Ag-SiN_x is observed, with the Ag-SiN_x layer thickness approximately 3 nm. The inverse fast Fourier transform (IFFT) pattern from region A in the Mo_2N layer, far from the Ag-SiN_x layer, is shown in Fig. 3(d). It reveals a series of lattice fringes with a spacing of around 0.247 nm, corresponding to fcc-Mo_2N (111) based on the JCPDF card # 25–1366. Although some regions in the Ag-SiN_x layer exhibit a fully amorphous characteristic without obvious lattice fringes, lattice fringes are still observed within this layer. These fringes extend throughout the layer, as indicated by the IFFT pattern in Fig. 3(e) from region B in Fig. 3(c), suggesting epitaxial growth of the Ag-SiN_x layer. The spacing of these fringes is around 0.241 nm, notably smaller than that within the Mo_2N layer (measured value of 0.247 nm in Fig. 3(d)). Significant distortions are observed in the pattern, indicating the influence of the epitaxial growth process.

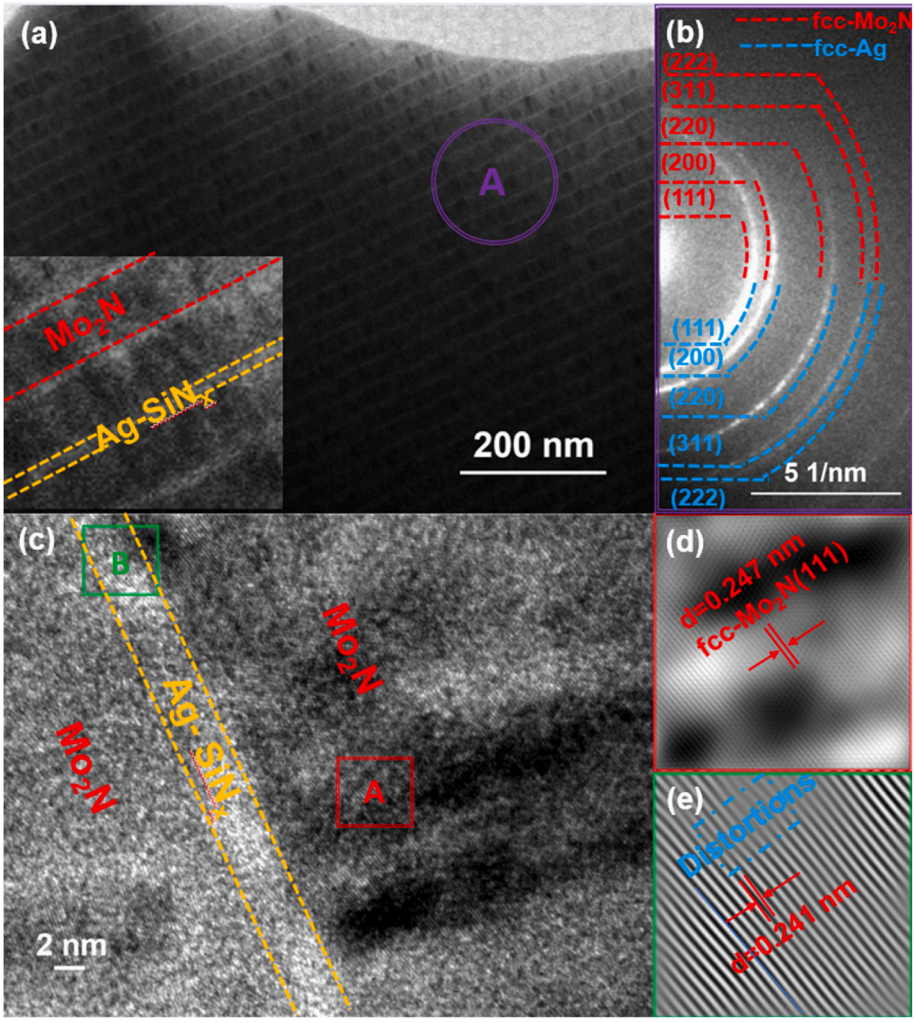

Fig. 3. The cross-sectional TEM image of the multilayered film with a modulation ratio of 1:9 (a), SAED pattern (b), HRTEM image (c), and its corresponding IFFT pattern from inner of Mo_2N layer (d), and the interfacial region with epitaxial characteristic (e).

Previous TEM studies have reported that Ag-SiN_x monolayered film exhibit a dual-phase structure of fcc-Ag and amorphous SiN_x, with Ag nano-particles embedded in the amorphous matrix [27]. The coherent structure induced by the soft metal epitaxial growth with the nitride-based template, exhibits a significant size dependence. For instance, the critical size of Ag epitaxial growing with the TiN template was reported to be below 4 nm, either for the Ag nano-particles in the TiN-Ag composite film, or for the Ag layers in the TiN/Ag nano-multilayered films [51]. The possibility of SiN_x growing with the nitride-based templates, such as Mo_2N, was also reported to be below 1 nm [40]. This experimental result was also confirmed by the calculation results [26]. Therefore, the coherent structure observed in the multilayered film could be attributed to the epitaxial growth of Ag nano-particles in the Ag-SiN_x layer on the Mo_2N template. This occurs when the critical thickness of the soft metal is around or below 3 nm. Consequently, this results in unique interfacial characteristics of the multilayered film, with a coherent structure between Ag and Mo_2N, and a mixed interface between amorphous SiN_x and Mo_2N crystalline. The regions exhibiting coherent structure characteristics lead to the reduction of the Mo_2N planes and the expansion of the Ag planes due to epitaxial growth and, thereby inducing the lattice distortions.

Based on above experimental results, the Mo_2N monolayered film exhibits a single phase of fcc- Mo_2N, while the Ag-SiN_x monolayer shows a dual-phase structure of Ag mixed with SiN_x. The multilayered films demonstrate a distinct alternating deposition of Mo_2N and Ag-SiN_x layers. When the modulation ratio is below 1:9, unique interfacial characteristic emerges, characterized by a coherent structure induced by the epitaxial growth of Ag within the Ag-SiN_x layer on the Mo_2N template. However, this kind of coherent structure disappears once the Ag-SiN_x layer thickness (modulation ratio above 1:9) is above the critical size of epitaxial growth of Ag in the nitride-based template.

3.2. Mechanical and tribological properties

The hardness and elastic modulus of the multilayered films with different modulation ratios are depicted in Fig. 4. The hardness of monolayered Mo_2N and Ag-SiN_x film is approximately 28 and 7 GPa, respectively. Alternating deposition of Mo_2N and Ag-SiN_x layers significantly influences the hardness of the multilayered films. Its maximum value reaches around 36 GPa for the modulation ratio of 1:9, whilst it gradually decreases with a further increase of the modulation ratio. The elastic modulus of the monolayered film of Mo_2N and Ag-SiN_x is about 260 and 105 GPa, respectively. The influential tendency of the elastic modulus of the multilayered films is similar as the one for the hardness: the value firstly increases to approximately 330 GPa for the film with a modulation ratio of 1:9, and then drops gradually from around 230 GPa for a modulation ratio of 1:6 to about 180 GPa for a modulation ratio of 1:1.

When compared to the hardness of the reference monolayered films, the multilayered film with a modulation period of 1:9 demonstrates a significant increase in hardness. This improvement is primarily attributed to the microstructural characteristics resulting from the epitaxy growth of Ag within the Ag-SiN_x layer alongside the Mo_2N template, and is given by two main reasons: First, the formation of a coherent interface occurs when Ag in the Ag-SiN_x layers grows epitaxially on the Mo_2N template, resulting in a continuous lattice structure across the interface. This slight lattice mismatch in coherent interfaces induces elastic strain in the layers [26]. Consequently, the strain field generated by this coherent structure can impede the movement of dislocations within the layers, making it more difficult for the film to deform. Second, these coherent interfaces act as barriers to dislocation motion [26]. Therefore, the presence of coherent interfaces enhances the hardness of the film by hindering the movement of dislocations. In addition, the alternating deposition of Mo_2N and Ag-SiN_x layers results in an increased number of interfaces, which makes it more difficult for dislocations to slip, thereby enhancing the hardness of the multilayer thin film material to a certain extent. However, once the size of the Ag exceeds the critical threshold for coherent growth, the coherent structure vanishes, causing a sharp decline in the hardness of the multilayer film with a modulation period greater than 1:9. At this stage, the hardness of the multilayered film decreases, approaching a value that closely reflects the volume-averaged hardness of the individual modulation layers.

The elastic modulus of the multilayer film with a modulation ratio of 1:9 also increases significantly, but the mechanism of its increase is different from that of hardness. The coherent structure characteristics cause the interplanar spacing to change, which changes the energy of adjacent bonds in the lattice, resulting in an increase in the elastic modulus. A further increase in the modulation ratio causes the elastic modulus of the multilayered films to decrease, which is the same trend as the hardness, with the value converging to the volume-averaged elastic modulus of the individual modulation layers.

Fig. 5 displays the room temperature average friction coefficient and wear rate for both Mo_2N and Ag-SiN_x monolayered films, as well as for Mo_2N/Ag-SiN_x multilayered ones with varying modulation ratios. As shown in Fig. 5(a), the average coefficients of friction of the Mo_2N and Ag-SiN_x monolayered films are 0.3 and 0.4, respectively. The average coefficients of friction of the Mo_2N/Ag-SiN_x multilayered films, with different modulation ratios, are higher than those of their monolayered ones and progressively increase with the modulation ratio, ranging from 0.42 at 1:9 to 0.58 at 1:1.

From Fig. 5(b), it is evident that the wear rates of the Mo_2N and Ag-SiN_x monolayered films are around 6.3×10^{-6} mm^3/N.mm, and 3.2×10^{-6} mm^3/N.mm, respectively. For the Mo_2N/Ag-SiN_x multilayer films, when the modulation ratio is 1:9, the multilayer film with a coherent structure demonstrates the best wear resistance. In comparison to the Mo_2N and Ag-SiN_x monolayered films, its wear rate at RT is reduced by an order of magnitude, reaching a value of about 1.9×10^{-7} mm^3/N.mm. As the modulation ratio increases, the wear rate of the multilayer film gradually increases, from approximately 8.3×10^{-7} mm^3/N.mm at a modulation ratio of 1:6 to around 3.4×10^{-6} mm^3/N.mm at a

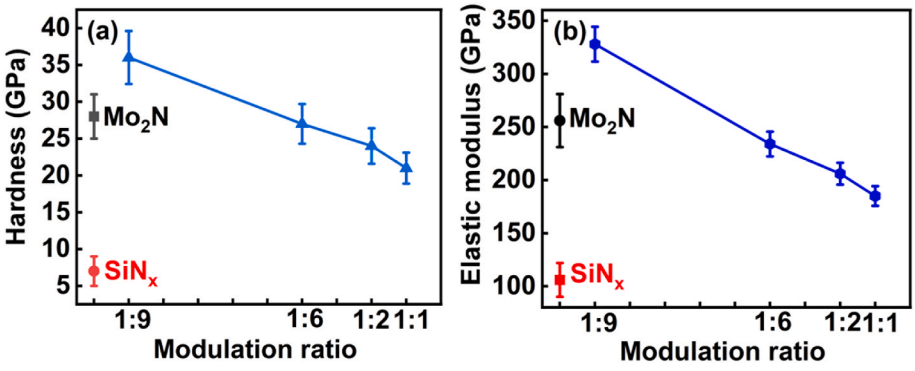

Fig. 4. Hardness (a) and elastic modulus (b) of the Mo_2N/Ag-SiN_x multilayered films as a function of modulation ratio of Ag-SiN_x to Mo_2N thickness.

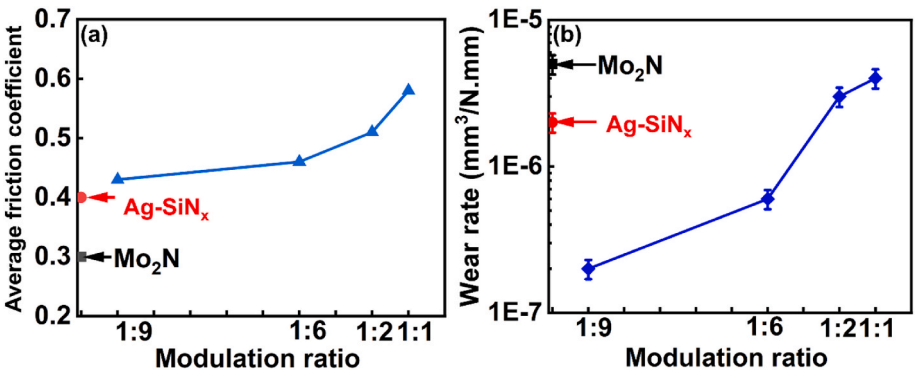

Fig. 5. Average coefficient of friction and wear rate of the Mo_2N/Ag-SiN_x multilayered films as a function of modulation ratio of Ag-SiN_x to Mo_2N thicknesses.

modulation ratio of 1:1.

Fig. 6 presents the optical microscopy images of the wear track on multilayer films with various modulation ratios, alongside their corresponding 2D morphologies. As illustrated in Fig. 6(a) and (b), the wear track width of the multilayer film with a modulation ratio of 1:9 is approximately 500 μm, with a maximum depth of about 1.5 μm. The wear track area exhibits a significantly darker color than the as-deposited one, indicating the occurrence of tribo-chemical reactions during tribo-testing, which likely led to the formation of friction phases. This observation was corroborated by subsequent Raman analysis (discussed in detail later), further confirming the presence and nature of these chemical transformations within the wear track region. In fact, it is not uncommon for nitride-based films to form tribo-chemical reaction tribo-phases under room temperature tribo-testing. For instance, the formation of layered tribo-phase MoO_3 with self-lubricating properties has been reported in multiple film systems such as Mo_2N [29], Mo_2N-Cu [18] and Mo_2N-Ag/SiN_x [24]. Distinct furrows are clearly visible on the surface of the wear track, with the majority concentrated in the center. These furrows are formed as a result of the load and shear forces exerted by the counterpart during the tribo-testing. Asperities on the wear track surface are crushed under this contact pressure from counterpart, and as the counterpart slides along the surface, hard debris embedded within these protrusions scratch the wear track, leading to the formation of the observed furrows. As the testing time increases, wear debris gathers ahead of the counterpart and slides along the wear track surface, resulting in the accumulation of debris on both sides of the wear track. Moreover, some areas on either side of the wear track peel off as they fracture under the pressure and shear forces during testing due to the films' brittleness. The wear track morphology of the multilayer film with a modulation ratio of 1:1 is shown in Fig. 6(c) and (d). Compared to the film with a modulation ratio of 1:9, the wear track's width increased to 1000 μm, while the wear track depth was approximately similar to that of the film with a modulation ratio of 1:9. However, deeper furrows were evident, with the deepest furrow reaching 2 μm. The film thickness under these conditions was 2 μm, indicating that the film had not worn out at this stage. The increased wear track width is primarily due to the

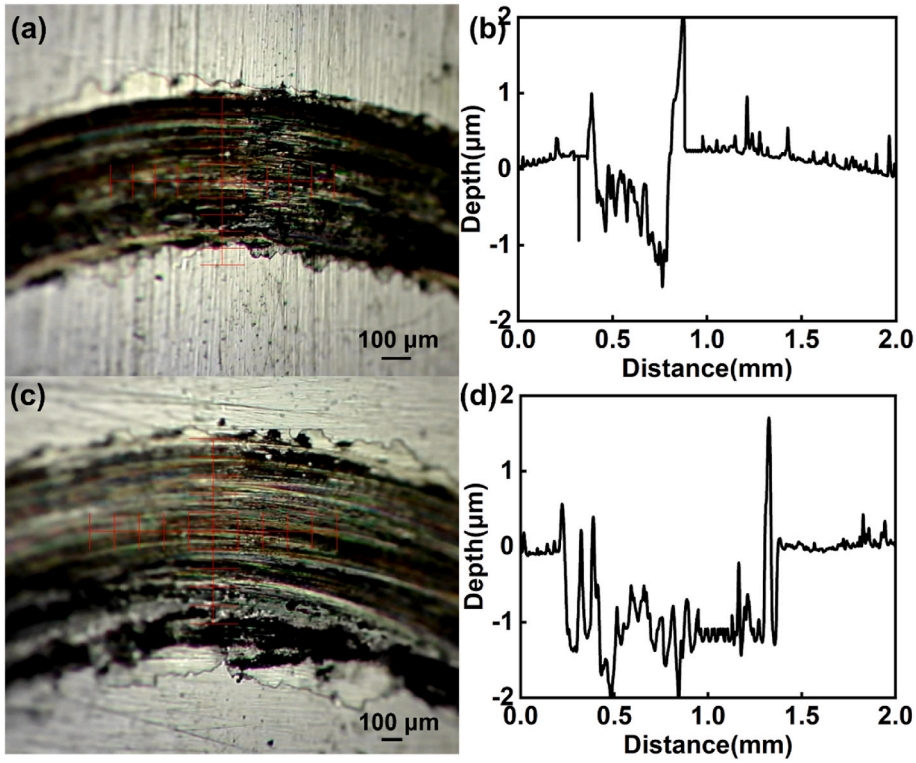

Fig. 6. Optical image of the wear track surface and its corresponding 2D curve of the Mo_2N/Ag-SiN_x multilayered films as a function of modulation ratio of Ag-SiN_x to Mo_2N thickness: (a, b) 1:9, (c, d) 1:1.

decreased film hardness (Fig. 6), which leads to a greater contact area and thus higher material removal during tribological testing. Similar to the wear track observed in the multilayer film with a modulation ratio of 1:9, the surface of the thin film wear track also appeared darker at this stage, consistent with previous analyses. The disappearance of the coherent structure resulted in disrupted interface continuity, making interlayer peeling more likely. Furthermore, the reduced hardness significantly contributed to the formation of deeper furrows on the wear track surface. The phenomenon of film peeling on both sides of the wear track was more pronounced compared to the 1:9 sample, further corroborating the aforementioned conclusion.

As shown in Fig. 7, the multilayer film with the lowest average friction coefficient and wear rate at RT (modulation ratio of 1:9) was taken as the research object, and the friction and wear performance were tested under RT-600 °C temperature cycle conditions. As can be seen from Fig. 7(a), in the first temperature cycle, the ambient temperature has a significant effect on the change of the friction curve: in RT-1, the friction curve enters a stable stage after a 400-s running stage, and the coefficient of friction stabilizes at 0.42, which is consistent with that in Fig. 5. In 600-1, after a short running-in period, the coefficient of friction stabilized at around 0.23, which was significantly lower than that of RT-1. In the second temperature cycle, the friction curve of RT-2 did not show an obvious running-in period, and the coefficient of friction was roughly stable at around 0.23, which was basically the same as that of 600-1. This could be attributed to the accumulation of a sufficient amount of lubricating phase during the friction process at 600-1, which effectively reduced wear resistance and maintained a consistently low coefficient of friction throughout the subsequent friction process at RT-2. During the friction process of 600-2, the coefficient of friction is similar to that of RT-2. During the third cycle, regardless of RT-3 or 600-3, the coefficient of friction remains relatively constant over time, stabilizing at approximately 0.2. Based on the above analysis, the average coefficients of friction under this temperature cycle condition are 0.42 (RT-1), 0.23 (600-1), 0.24 (RT-2), 0.23 (600-2), 0.22 (RT-3), and 0.20 (600-3).

Fig. 7(b) shows the 2D morphology of the wear track under the temperature cycle condition. It can be seen that after the RT-1 friction test, the depth and width of the wear track are approximately 1.5 and 500 μm, respectively. Obvious furrows appeared in the center of the wear track, and there was accumulation of wear debris on both sides of the wear track. These phenomena are similar to those observed in Fig. 5. Then, after the first temperature cycle of the 600 °C (600-1) friction test, a large amount of friction products adhered to the wear track surface, reflecting the negative wear phenomenon, and the actual wear rate could not be measured. After the RT-2 friction test, although the height of the friction products on the wear track decreased, it still showed negative wear, and the actual wear rate was still unmeasurable. After the 600-2 experiment, the adhesion products increased significantly, and so the wear track height increased significantly, which also confirmed that a large number of adhesion products were easily produced in the tribological environment at 600 °C. During the third temperature cycle, the wear track surface exhibited a trend similar to that observed during the second cycle. A significant amount of adhesive products adhered to the wear track surface, and the actual wear rate was unmeasurable.

From the friction and wear experiments under the above RT-600 °C temperature cycle conditions, it can be seen that, except for the first room temperature friction test, the film has shown a stable and low coefficient of friction, maintaining a value around 0.2, and has excellent wear resistance. Even after three temperature cycles, a significant amount of wear debris remains adhered to the wear surface, making the wear rate unpredictable.

Fig. 8 shows the Raman spectra of the wear track surface after each temperature cycle tribological test. After the first room temperature friction test (RT-1), the Raman spectrum of the wear track showed four weak peaks at 380, 670, 953 and 1000 cm^{-1}. Among them, the first two correspond to MoO_3 and the last two correspond to Ag_2MoO_4. After the first temperature cycle of 600 °C (600-1), the peaks in the Raman spectrum from the wear track are significantly improved in both quantity and intensity compared with RT-1. Among them, those at 315, 337, 661 cm^{-1} correspond to MoO_3 [41,42]; at 721, 810, 1001 cm^{-1}, to Ag_2MoO_4 [43,44]; at 903 cm^{-1}, to $Ag_2Mo_4O_{13}$ [45,46]; at 500 cm^{-1}, to $Ag_2Mo_2O_7$ [47,48]; and at 401 cm^{-1} to SiO_2 [49]. Subsequently, after tribo-testing at both room temperature and 600 °C, distinct peaks corresponding to the aforementioned five friction phases emerge in the Raman spectrum of the wear track. Although room temperature friction

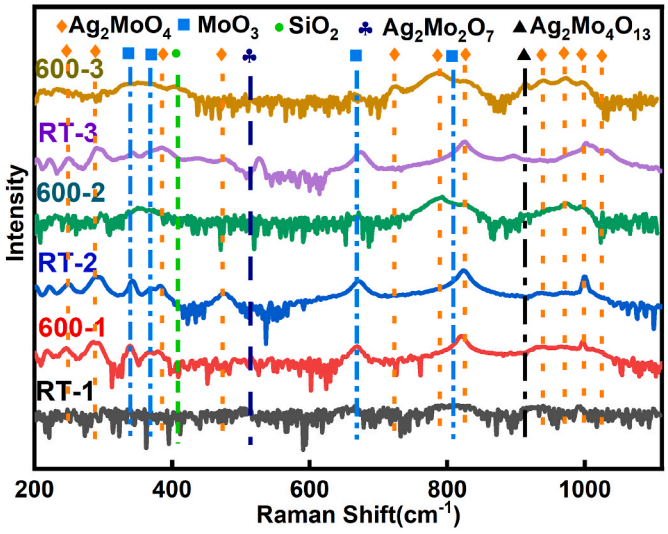

Fig. 8. Raman spectra from the wear track after each cycling of the RT-600 temperature cycling tribo-testing.

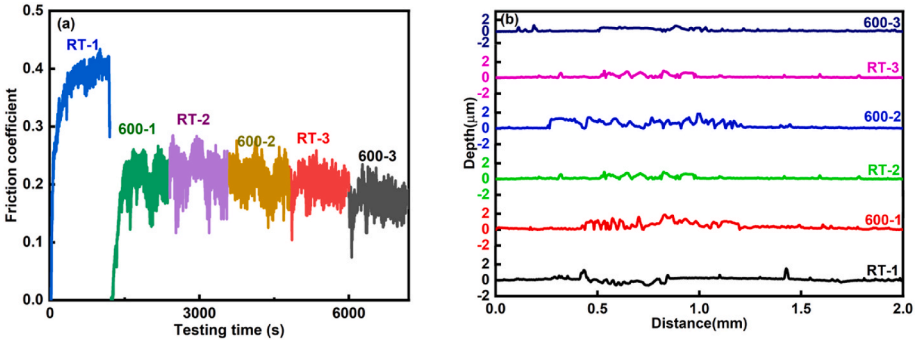

Fig. 7. Friction curves (a), 2D wear track morphologies (b) of the multilayered film with a modulation ratio of 1:9 after the RT-600 °C temperature-cycling tribo-testing.

generally does not induce significant chemical reactions on the wear track surface, as indicated by the Raman results of RT-1, a substantial amount of products remains in the wear track after the initial temperature cycle following friction at 600 °C. This accumulation is the main factor contributing to the prominent friction phases observed on the wear track surfaces of RT-2 and RT-3.

Based on the above experimental result, the room temperature friction behavior of multilayer films with different modulation ratios indicates that the average coefficient of friction gradually increases with higher modulation ratios. However, across all modulation ratios, the average coefficient of friction is consistently higher than that of Mo_2N and Ag-SiN_x single-layer films. When the modulation ratio is 1:9, the hardness of the film is the highest. During the tribo-testing, under the action of the counterpart, the hard abrasive particles, under the action of the grinding pair, scratch the surface of the wear mark, creating distinct furrows. This results in intense interaction between the two surfaces between the counterpart and wear track. Therefore, its average coefficient of friction is higher than that of Mo_2N and Ag-SiN_x monolayered films. As the modulation ratio increases, the hardness gradually decreases, which results in the contact area between the wear track and the counterpart increases gradually, leading to higher frictional forces and thus a gradual increase in the average coefficient of friction. The multilayered film with a modulation ratio of 1:9 exhibits a coherent structure with continuous interfaces between the layers, which effectively avoid interlayer delamination. Moreover, the formation of a coherent structure can significantly strengthen the film by improving both hardness and toughness, thereby enhancing its load-bearing capacity and resistance to crack initiation and propagation. Thereby, the film's wear resistance greatly improves and the wear resistance is increased by an order of magnitude compared to the two single-layer films. When the modulation ratio is higher than 1:9, the thickness of the Ag-SiN_x layer exceeds the critical size of the coherent structure. Consequently, the mechanical properties of the multilayer film material tend to follow the law of mixing more closely, reducing its hardness and gradually increasing the film's wear rate. Despite detecting solid-lubricant friction-reducing products, like MoO_3, in the wear track, their presence is reduced. Therefore, the microstructure of the multilayer film and the resulting changes in mechanical properties have a more significant impact on the friction and wear characteristics at room temperature. Moreover, the multilayered architecture—particularly with a modulation ratio of 1:9—promotes the formation of coherent interlayers. This structural coherence, along with the associated mechanical strengthening and the elimination of distinct interfacial boundaries, leads to improved tribological performance compared to the Mo_2N–Ag–SiN_x composite system [50].

Regarding the friction and wear resistance properties of the multilayer film with a modulation ratio of 1:9 under temperature cycling from RT to 600 °C, the behavior observed during the initial cycle at RT aligns with the earlier discussion in the RT tribological section. In the subsequent 600-1 cycle, SiN_x demonstrates a significant sustained release of Ag at elevated temperatures, continuing the slow release of the Ag lubricating agent [24,25]. However, the adhesion of tribo-phases caused by the counterpart and the expansion of volume induced by tribo-oxidation make it impossible to calculate the wear rate. The emergence of a lubricating tribo-phase is indicated by the film maintaining a stable average coefficient of friction of around 0.2. Despite a substantial amount of the lubricious tribo-phase adhering to the worn surface, the average coefficient of friction at room temperature (RT-2) remains steady at 0.2, and the actual wear rate cannot be measured. The friction behaviour observed in 600-2 and 600-3 mirrors that of 600-1, while the friction behaviour in RT-3 is similar to that in RT-2. Therefore, since 600-1, the average coefficient of friction of the multilayer film has remained stable at about 0.2, and the wear rate is still impossible to calculate owning to the adhesion of tribo-phase as well as the volume expansion.

4. Conclusion

Nowadays, achieving simultaneous enhancement of both mechanical and self-lubricating properties by alloying soft lubricant agents into nitrides remains a significant challenge. This study focuses on the development and optimization of wide-range temperature self-lubricating films, specifically novel RF magnetron-sputtered Mo_2N/Ag-SiN_x multilayered films. These films were designed with a fixed modulation period of 30 nm and varied modulation ratios (γ) to achieve long-term lubrication while maintaining excellent mechanical properties. The main findings of the study are as follows.

(1) The multilayered film consists of two distinct layers: Mo_2N and Ag-SiN_x. The Mo_2N layer exhibited a single fcc-Mo_2N phase, while the Ag-SiN_x layer displayed a dual-phase structure, comprising fcc-Ag nanoparticles and an amorphous SiN_x matrix. At a γ of 1:9, the Ag-SiN_x layer grew epitaxially on the Mo_2N template, forming a coherent structure. However, this coherent structure diminished as γ increased.
(2) The microstructure of the multilayered films significantly influenced their mechanical properties. The coherent structure at γ of 1:9 enhanced both hardness and elastic modulus, reaching approximately 36 GPa and 230 GPa, respectively, due to coherency strengthening.
(3) The wear rate of the multilayered film at room temperature also benefited from the coherent structure, which enhanced mechanical properties. The wear rate for the film with γ of 1:9 dropped to around 8.3×10^{-7} mm^3/N.mm. However, the low-friction properties were not significantly improved by this structural design.
(4) During three RT-600 °C temperature cycles, the multilayered film with γ of 1:9 maintained a stable coefficient of friction around 0.2, except for the first room temperature tribological test, where it was 0.4. The excellent temperature-cycling tribological properties were attributed to the synergistic lubricant characteristics of both layers and the formation of self-lubricating tribo-phases.

This study demonstrated that the optimized Mo_2N/Ag-SiN_x multilayered films can provide effective solid-lubrication and mechanical stability under extreme conditions, achieving the mutually enhanced mechanical and tribological properties, offering a promising solution for high-performance engineering applications.

CRediT authorship contribution statement

Jing Luan: Data curation, Investigation, Writing – original draft. **Lei Wang:** Methodology, Software, Validation, Writing – review & editing. **Songtao Dong:** Investigation, Methodology. **Filipe Fernandes:** Supervision. **Andrei Choukourov:** Investigation, Methodology. **Junfeng Yang:** Investigation, Methodology. **Mitjan Kalin:** Supervision. **Albano Cavaleiro:** Supervision, Methodology, Writing – review & editing. **Hongbo Ju:** Writing – review & editing, Writing – original draft, Visualization, Validation, Supervision, Resources, Project administration, Methodology, Investigation, Funding acquisition, Formal analysis, Data curation, Conceptualization.

Declaration of competing interest

We declare that we do not have any commercial or associative interest that represents a conflict of interest in connection with the work submitted.

Acknowledgement

Supported by the projects granted by the National Natural Science Foundation of China with the number of 52171071 and 51801081,

national funds through FCT of Portugal – Fundação para a Ciência e a Tecnologia, under a scientific contract of 2021.04115. CEECIND, 2023.06224.CEECIND, under projects UID/00285- Centre for Mechanical Engineering, Materials and Processes, LA/P/0112/2020, Slovenian Research Agency ARIS under the Research Core Funding Programme No. P2-0231 and the Marie Skłodowska-Curie Actions (MSCA) with the number of MSCA-COFUND-5100-237/2023-9. Prof. H. Ju's student - F. Kong also acknowledged the Post-graduate Research Innovative Training Program Jiangsu Province of China, with a number of SJCX23_2190.

References

[1] A. Erdemir, A crystal-chemical approach to lubrication by solid oxides, Tribol. Lett. 8 (2000) 97–102.
[2] S. Zhu, J. Cheng, Z. Qiao, J. Yang, High temperature solid-lubricating materials: a review, Tribol. Int. 133 (2019) 206–223.
[3] H. Ju, M. Athmani, J. Luan, A. Al-Rjoub, A. Cavaleiro, T.B. Yaqub, A. Chala, F. Ferreira, F. Fernandes, Insights into the oxidation resistance mechanism and tribological behaviors of multilayered TiSiN/CrV_xN hard coatings, Int. J. Miner. Metall. Mater. 30 (2023) 2459–2468.
[4] S.M. Aouadi, B. Luster, P. Kohli, C. Muratore, A.A. Voevodin, Progress in the development of adaptive nitride-based coatings for high temperature tribological applications, Surf. Coating. Technol. 204 (2009) 962–968.
[5] H. Ju, P. Jia, J. Xu, L. Yu, A. Issac, Crystal structure and high temperature tribological behavior of niobium aluminum nitride films, Materialia 3 (2018) 202–211.
[6] C.G. Guleryuz, J.E. Krzanowski, S.C. Veldhuis, G.S. Fox-Rabinovich, Machining performance of TiN coatings incorporating indium as a solid lubricant, Surf. Coating. Technol. 203 (2009) 3370–3376.
[7] H. Ju, L. Yu, D. Yu, I. Asempah, J. Xu, Microstructure, mechanical and tribological properties of TiN-Ag films deposited by reactive magnetron sputtering, Vacuum 141 (2017) 82–88.
[8] Y. Ren, J. Jia, X. Cao, G. Zhang, Q. Ding, Effect of Ag contents on the microstructure and tribological behaviors of NbN-Ag coatings at elevated temperatures, Vacuum 204 (2022) 111330.
[9] H. Ju, N. Ding, J. Xu, L. Yu, Y. Geng, G. Yi, T. Wei, Improvement of tribological properties of niobium nitride films via copper addition, Vacuum 158 (2018) 1–5.
[10] S.M. Aouadi, D.P. Singh, D.S. Stone, K. Polychronopoulou, F. Nahif, C. Rebholz, C. Muratore, A.A. Voevodin, Adaptive VN/Ag nanocomposite coatings with lubricious behavior from 25 to 1000 °C, Acta Mater. 58 (2010) 5326–5331.
[11] H. Ju, Pei Jia, J. Xu, L. Yu, Y. Geng, Y. chen, M. Liu, T. Wei, The effects of adding aluminum on crystal structure, mechanical, oxidation resistance, friction and wear properties of nanocomposite vanadium nitride hard films by reactive magnetron sputtering, Mater. Chem. Phys. 215 (2018) 368–375.
[12] X. Xu, J. Sun, F. Su, Z. Li, Y. Chen, Z. Xu, Microstructure and tribological performance of adaptive MoN-Ag nanocomposite coatings with various Ag contents, Wear 488–489 (2022) 204170.
[13] G. Wu, F. Song, Y. Shi, B. Yu, J. Pu, Y. Wang, Effect of multi-doping on the tribological behavior of MoN(Ag)-based films in a wide temperature range, Mater. Sci. 58 (2023) 3960–3971.
[14] J. Li, D. Xiong, H. Wu, H. Zhu, J. Kong, R. Tyagi, Tribological properties of MoN layer on silver-containing nickel-base alloy at high temperatures, Wear 271 (2011) 987–993.
[15] T. Rasheed, A.A. Sorour, Unveiling the power of MXenes: solid lubrication perspectives and future directions, Adv. Colloid Interface Sci. 329 (2024) 103186.
[16] A.A. Voevodin, C. Muratore, S.M. Aouadi, Hard coatings with high temperature adaptive lubrication and contact thermal management: review, Surf. Coating. Technol. 257 (2014) 247–265.
[17] H. Ju, D. Yu, L. Yu, N. Ding, J. Xu, X. Zhang, Y. Zheng, L. Yang, X. He, The influence of Ag contents on the microstructure, mechanical and tribological properties of ZrN-Ag films, Vacuum 148 (2018) 54–61.
[18] H. Ju, R. Zhou, S. Liu, L. Yu, J. Xu, Y. Geng, Enhancement of the tribological behavior of self-lubricating nanocomposite Mo_2N/Cu films by adding the amorphous SiN_x, Surf. Coating. Technol. 423 (2021) 127565.
[19] Y. Dong, Z. Wang, J. Yuan, Z. Wang, Y. Zhang, G. Ma, A. Wang, Temperature-adaptive lubrication of Ag doped Cr_2AlC nanocomposite coatings, Wear 540–541 (2024) 205221.
[20] J. Luan, F. Kong, M. Evaristo, F. Fernandes, Y. Zhou, A. Cavaleiro, H. Ju, Design and magnetron sputtering of nanomultilayered W_2N/Ag-SiN_x films: microstructural insights and optimized self-lubricant properties from room temperature to 500 °C, Ceram. Int. 50 (20) (2024) 39226–39234.
[21] W. Wang, J. Pu, Z. Cai, S. Zheng, Y. Wei, Insights into friction properties and mechanism of self-lubricating MoVN-Ag films at high temperature, Vacuum 176 (2020) 109332.
[22] H. Ju, X. He, L. Yu, J. Xu, The microstructure and tribological properties at elevated temperatures of tungsten silicon nitride films, Surf. Coating. Technol. 326 (2017) 255–263.
[23] J. Ding, T. Zhang, J. Yun, K. Kim, Q. Wang, Effect of Cu addition on the microstructure and properties of TiB_2 films deposited by a hybrid system combining high power impulse magnetron sputtering and pulsed dc magnetron sputtering, Surf. Coating. Technol. 344 (2018) 441–448.
[24] H. Ju, R. Zhou, J. Luan, L. Yu, J. Xu, B. Zuo, J. Yang, Y. Geng, L. Zhao, F. Fernandes, Multilayer Mo_2N-Ag/SiN_x films for demanding applications: morphology, structure and temperature-cycling tribological properties, Mater. Des. 223 (2022) 111128.
[25] H. Ju, J. Guo, L. Yu, J. Xu, J. Luan, Enhancement of the mechanical and tribological properties of self-lubricant Mo_2N-Ag composite film by adding amorphous SiN_x, Ceram. Int. 50 (2024) 8463–8471.
[26] H. Ju, J. Luan, Y. Wang, A. Bondarev, M. Evaristob, Y. Geng, J. Xu, A. Cavaleiro, F. Fernandes, Mutual promotion on the mechanical and tribological properties of the nacre-like self-lubricant film designed for demanding green tribological applications, Friction 13 (3) (2025) 9440963.
[27] H. Ju, K. Huang, J. Luan, Y. Geng, J. Yang, J. Xu, Evaluation under temperature cycling of the tribological properties of Ag-SiN_x films for green tribological applications, Ceram. Int. 49 (2023) 30115–30124.
[28] C. Liu, H. Ju, J. Xu, L. Yu, Z. Zhao, Y. Geng, Y. Zhao, Influence of copper on the compositions, microstructure and room and elevated temperature tribological properties of the molybdenum nitride film, Surf. Coating. Technol. 395 (2020) 125811.
[29] C. Liu, H. Ju, L. Yu, J. Xu, Y. Geng, W. He, J. Jiao, Tribological properties of Mo_2N films at elevated temperature, Coatings 9 (2019) 734.
[30] C. Sarioglua, U. Demirlerb, M. Kazmanlib, M. Urgenb, Measurement of residual stresses by X-ray diffraction techniques in MoN and Mo_2N coatings deposited by arc PVD on high-speed steel substrate, Surf. Coating. Technol. 190 (2005) 238–243.
[31] K. Pappacena, D. Singh, O. Ajayi, J. Routbort, O. Erilymaz, N. Demas, G. Chen, Residual stresses, interfacial adhesion and tribological properties of MoN/Cu composite coatings, Wear 278–279 (2012) 62–70.
[32] B. Bouaouina, A. Besnard, S.E. Abaidia, F. Haid, Residual stress, mechanical and microstructure properties of multilayer Mo_2N/CrN coating produced by R.F magnetron discharge, Appl. Surf. Sci. 395 (2017) 117–121.
[33] L. Zhang, H. Yang, X. Pang, K. Gao, A. Volinsky, Microstructure, residual stress, and fracture of sputtered TiN films, Surf. Coating. Technol. 224 (2013) 120–125.
[34] J. Luan, H. Lu, J. Xu, F. Fernandes, M. Evaristo, B. Ma, F. Xie, A. Cavaleiro, H. Ju, Exploring tribological characteristics of ZrN-MoSN composite films fabricated via RF magnetron sputtering: insights from microstructure and performance analysis, Surf. Coating. Technol. 484 (2024) 130813.
[35] Z. Rao, E. Chason, Measurements and modeling of residual stress in sputtered TiN and ZrN: dependence on growth rate and pressure, Surf. Coating. Technol. 404 (2020) 126462.
[36] R. Abdullaev, R. Khairulin, S. Stankus, Density and thermal expansion of silver in the solid and liquid states, J. Phys. Conf. 1677 (2020) 012161.
[37] Q. Zhang, J. Ge, B. Zhang, C. He, Z. Wu, J. Liang, Effect of thermal residual stress on the tensile properties and damage process of C/SiC composites at high temperatures, Ceram. Int. 48 (2022) 3109–3124.
[38] S. Bogatyrenko, A. Kryshtal, Thermal expansion coefficients of Ag, Cu and diamond nanoparticles: in situ TEM diffraction and EELS measurements, Mater. Char. 178 (2021) 111296.
[39] H. Ju, J. Luan, J. Xu, A. Cavaleiro, M. Evaristo, F. Fernandes, Nano-multilayered ZrN-Ag/Mo-S-N film design for stable anti-frictional performance at a wide range of temperatures, Friction 12 (12) (2024) 2826–2837.
[40] G. Zhang, T. Fan, T. Wang, H. Chen, Microstructure, mechanical and tribological behavior of MoN_x/SiN_x multilayer coatings prepared by magnetron sputtering, Appl. Surf. Sci. 274 (2013) 231–236.
[41] E. Santos, F. Sigoli, I. Mazali, Study of structure of the TiO_2-MoO_3 bilayer films by Raman spectroscopy, Mater. Res. Bull. 60 (2014) 242–246.
[42] P. Chelvanathan, K. Rahman, M. Hossain, H. Rashid, N. Samsudin, S. Mustafa, B. Bais, M. Akhtaruzzaman, N. Amin, Growth of MoO_x nanobelts from molybdenum bi-layer thin films for thin film solar cell application, Thin Solid Films 621 (2017) 240–246.
[43] J. Yang, J. Jia, X. Li, C. Lu, X. Feng, Synergistic lubrication of Ag and Ag_2MoO_4 nanoparticles anchored in plasma-sprayed YSZ coatings: remarkably-durable lubricating performance at 800 °C, Tribol. Int. 153 (2021) 106670.
[44] D. Wang, H. Tan, W. Chen, S. Zhu, J. Cheng, J. Yang, Tribological behavior of Ni3Al-Ag based self-lubricating alloy with Ag_2MoO_4 formed by high temperature tribo-chemical reaction, Tribol. Int. 153 (2021) 106659.
[45] X. Dai, M. Wen, K. Huang, X. Wang, L. Yang, J. Wang, K. Zhang, Toward low friction in water for Mo_2N/Ag coatings by tailoring the wettability, Appl. Surf. Sci. 447 (2018) 886–893.
[46] Q. Zhang, A. Goldbach, N. Ta, W. Shen, Selective oxidation of propylene to acrolein over silver-promoted hexagonal molybdates and derivative Ag/$Ag_2Mo_4O_{13}$/α-MoO_3 composites, Appl. Catal. Gen. 623 (2021) 118275.
[47] B. Sun, F. Ding, B. Qiu, Y. Zhao, J. Guo, High temperature tribological properties of NiAl-$Ag_2Mo_2O_7$ composite coatings prepared by spark plasma sintering, Surf. Coating. Technol. 456 (2023) 129290.
[48] A. Ferreira, W. Ferreira, A. Duarte, C. Santos, P. Freire, C. Luz-Lima, J. Moura, In situ high-temperature Raman scattering study of monoclinic $Ag_2Mo_2O_7$ microrods, Spectrochim. Acta Mol. Biomol. Spectrosc. 295 (2023) 122632.
[49] L. Rocha-Arredondo, J. Ortega-Gallegos, J. Flores-Camacho, R. Balderas-Navarro, Raman study of directly synthetized graphene oxide films on Si, SiO_2/Si and GaAs by remote-catalyzed CVD, Phys. B Condens. Matter 669 (2023) 415302.
[50] H. Ju, J. Guo, L. Yu, J. Xu, J. Luan, Enhancement of the mechanical and tribological properties of self-lubricant Mo_2N–Ag composite film by adding amorphous SiN_x, Ceram. Int. 50 (5) (2024) 8463–8471.
[51] J. Luan, F. Kong, J. Xu, F. Fernandes, M. Evaristo, S. Dong, A. Cavaleiro, H. Ju, Deciphering the mechanical strengthening mechanism: Soft metal doping in ceramic matrices-A case study of TiN-Ag films, Mater. Des. 248 (2024) 113489.